

# Bench-Top Method for Fabricating Glass-Sealed Nanodisk Electrodes, Glass Nanopore Electrodes, and Glass Nanopore Membranes of Controlled Size

Bo Zhang,<sup>†,‡</sup> Jeremy Galusha,<sup>†</sup> Peter G. Shiozawa,<sup>†</sup> Gangli Wang,<sup>†</sup> Adam Johan Bergren,<sup>§,||</sup> Ronald M. Jones,<sup>†</sup> Ryan J. White,<sup>†</sup> Eric N. Ervin,<sup>†</sup> Chris C. Cauley,<sup>†</sup> and Henry S. White<sup>\*,†</sup>

Department of Chemistry, University of Utah, 315 S, 1400 E, Salt Lake City, Utah 84112, and  
Department of Chemistry, Iowa State University, Ames, Iowa 50011

A simple benchtop method of fabricating glass-sealed nanometer-sized Au and Pt disk electrodes, glass nanopore electrodes, and glass nanopore membranes is reported. The synthesis of all three structures is initiated by sealing the tips of electrochemically sharpened Au and Pt microwires into glass membranes at the end of a soda lime or lead glass capillary. Pt and Au nanodisk electrodes are obtained by hand polishing using a high-input impedance metal oxide semiconductor field effect transistor (MOSFET)-based circuit to monitor the radius of the metal disk. Proper biasing of the MOSFET circuit, based on a numerical analysis of the polishing circuit impedance, allows for the reproducible fabrication of Pt disk electrodes of radii as small as 10 nm. Significantly smaller background currents in voltammetric measurements are obtained using lead glass capillaries, a consequence of the lower mobility of  $\text{Pb}^{2+}$  (relative to  $\text{Na}^+$ ) in the glass matrix. Glass nanopore electrodes and glass nanopore membranes are fabricated, respectively, by removal of part or all of the metal sealed in the glass membranes. The nanostructures are characterized by atomic force microscopy, steady-state voltammetry, and ion conductivity measurements.

In this report, we describe a simple benchtop method of reproducibly fabricating (i) glass-sealed Au and Pt nanodisk electrodes, (ii) glass nanopore electrodes, and (iii) glass nanopore membranes. These three nanostructures, schematically depicted in Figure 1, share common fabrication steps that have been outlined in preliminary reports from our laboratory.<sup>1–5</sup> Briefly, the

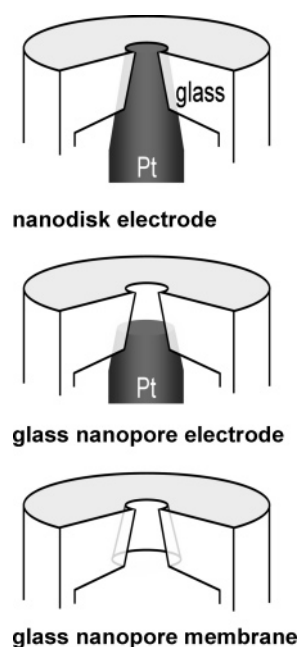


**Figure 1.** Schematic drawings of (A) nanodisk electrode, (B) glass nanopore electrode, and (C) glass nanopore membrane. The structures are not drawn to scale.

fabrication of a disk electrode involves sealing an electrochemically sharpened Au or Pt microwire into a glass capillary, followed by polishing the glass until a nanometer-sized metal disk is exposed. The fabrication of a glass nanopore electrode is accomplished by etching the metal nanodisk electrode to create a pore in glass, with the remaining metal disk comprising the pore base. Complete removal of the wire yields a glass nanopore membrane, in which a conical-shaped pore is embedded in a thin ( $\sim 50 \mu\text{m}$ ) glass membrane. Herein, we provide previously unpublished details of the fabrication and characterization of these nanostructures.

The use of nanometer-scale electrodes (radius between 1 and 100 nm) has attracted considerable interest as tools in fundamental research since the late 1980s. For example, electrodes of nanometer dimensions have been employed in studies of fast electron-transfer reactions,<sup>6,7</sup> interfacial structure,<sup>8–15</sup> single-electron and

\* Corresponding author: (e-mail) white@chem.utah.edu.

<sup>†</sup> University of Utah.

<sup>‡</sup> Present address: Department of Chemistry, Pennsylvania State University, 104 Chemistry Building, University Park, PA 16802.

<sup>§</sup> Iowa State University.

<sup>||</sup> Present address: National Institute for Nanotechnology, University of Alberta, Edmonton, Alberta, Canada.

(1) Zhang, B.; Zhang, Y. H.; White, H. S. *Anal. Chem.* **2004**, *76*, 6229.

(2) Zhang, B.; Zhang, Y. H.; White, H. S. *Anal. Chem.* **2006**, *78*, 477.

(3) Zhang, Y. H.; Zhang, B.; White, H. S. *J. Phys. Chem. B* **2006**, *110*, 1768.

(4) Wang, G.; Zhang, B.; Wayment, J. R.; Harris, J. M.; White, H. S. *J. Am. Chem. Soc.* **2006**, *128*, 7679.

(5) White, R. J.; Zhang, B.; Daniel, S.; Tang, J. M.; Ervin, E. N.; Cremer, P. S.; White, H. S. *Langmuir* **2006**, *22*, 10777.

(6) Watkins, J. J.; Chen, J.; White, H. S.; Abruña, H. D.; Maisonhaute, E.; and Amatore, C. *Anal. Chem.* **2003**, *75*, 3962.

single-molecule electrochemistry,<sup>16</sup> and as mimics of fuel cell catalysts.<sup>17</sup> Moreover, nanometer-scale electrodes find applications as scanned probe tips in scanning electrochemical microscopy,<sup>18–20</sup> and electrochemical atomic force<sup>21</sup> and tunneling microscopies<sup>22</sup> and as analytical probes in bioelectrochemical measurements.<sup>23</sup> In addition to conventional electrochemical measurements using the nanodisk electrodes, chemically modified glass nanopore electrodes have been employed to study molecular transport through nanometer-scale orifices,<sup>4</sup> while glass nanopore membranes have been used as solid supports for lipid bilayers.<sup>5</sup> A number of recent reports have described alternative methods, e.g., focused ion beam milling, embedded carbon nanotubes, etc., of preparing nanopore electrodes and nanopore membranes for applications in chemical analyses.<sup>24,25</sup>

Methods of fabricating nanometer-sized electrodes can be found in several reports,<sup>26,27</sup> including an excellent recent review by Arrigan.<sup>28</sup> Most frequently, and beginning with the work of Penner et al.,<sup>7</sup> the end of an electrochemically etched carbon fiber or metal wire is sealed into an insulating material (e.g., glass,<sup>29,30</sup> wax,<sup>31</sup> and polymers<sup>32,33</sup>) leaving the tip of the fiber or wire exposed. Electrodes fabricated in this way generally have a hemispherical or conical shape and are shrouded by a thin layer of insulating material. Although ideally inert, the nature of the

insulator can restrict the use of the electrode. For example, electrodes insulated with thin organic layers are simple to prepare, but their use is generally restricted to aqueous solutions, and they tend to exhibit prohibitively large capacitive currents in transient measurements due to the capacitance of the thin insulating layer.<sup>6</sup>

Nanometer-scale disk electrodes have been fabricated by first pulling Pt wires embedded in glass capillaries with micropipet pullers and subsequently exposing a disk-shaped area of the metal using mechanical polishes or chemical etchants.<sup>14,34</sup> The resulting glass-shrouded electrodes are very durable (their surface can be regenerated by polishing) and have favorable electrical properties. However, using these procedures, it is difficult to prepare electrodes with consistent sizes. Moreover, the use of costly pipet pullers is required.

In this report, a method for preparing Pt and Au nanodisk electrodes is detailed that utilizes hand polishing of a glass capillary after embedding a sharpened metal wire in the capillary. The key to the success of this methodology is the use of a high-input impedance metal oxide semiconductor field effect transistor (MOSFET)-based circuit to monitor the radius of the disk electrode during polishing. Shao and Mirkin briefly mentioned the use of an electrical continuity circuit in preparation of glass-sealed Pt nanoelectrodes<sup>14</sup> but did not report any details of their method. Herein, we discuss the proper biasing of the MOSFET circuit, based on a detailed understanding of the polishing circuit impedance, which enables the routine, benchtop fabrication of Pt nanodisk electrodes of preselected radius as small as ~10 nm. These metal disk electrodes are the starting point for fabrication of glass nanopore electrodes and glass nanopore membranes, which is also described in this report.

## EXPERIMENTAL SECTION

**Chemicals.** Ferrocene (100%, Alfa Aesar), reagent grade H<sub>2</sub>SO<sub>4</sub> (Fisher), NaCN, NaOH, and acetone (Mallinckrodt Chemicals) were used as received without further purification. Tetra-*n*-butylammonium hexafluorophosphate (TBAPF<sub>6</sub>, Aldrich) was recrystallized from absolute ethanol (Aaper) and dried under vacuum. HPLC-grade acetonitrile (Sigma-Aldrich) was stored over 3-Å molecular sieves. Water (>18 MΩ·cm) was obtained from a Barnstead E-pure water purification system. Gamma alumina particles (50 nm, Buehler) were used as received.

**Fabrication of Nanoelectrodes.** The 25-, 50-, and 100-μm-diameter Pt (99.95%) and 50-μm-diameter Au (99.99%) wires were obtained from Alfa-Aesar. Three types of glass capillaries were used in fabricating electrodes: (i) Dagan Corp. SB16 (1.65-mm o.d., 0.75-mm i.d., softening point 700 °C, manufacturer provided composition 67.7% SiO<sub>2</sub>, 2.8% BaO, 15.6% Na<sub>2</sub>O, 5.6% CaO, 4% MgO, 1.5% B, and 0.6% K<sub>2</sub>O); (ii) World Precision Instruments, Inc. PG10150-4 (1.5-mm o.d., 0.75-mm i.d., softening point ~625 °C, 22% PbO, other components unspecified); and (iii) Corning 8161 Patch Clamp Glass (1.50-mm o.d., 1.10-mm i.d., softening point 600 °C, composition 51% PbO, 39% SiO<sub>2</sub>, 6% K<sub>2</sub>O, 2% BaO). Type i capillaries, which contain predominantly SiO<sub>2</sub>, are referred to hereafter as soda lime glass capillaries. Types ii and iii capillaries, with significant Pb content, are referred to as Pb-doped glass capillaries.

A 2-cm length of Pt or Au wire was connected to a W rod using Ag conductive epoxy (DuPont). The Pt/W or Au/W ensemble

- (7) Penner, R. M.; Heben, M. J.; Longin, T. L.; Lewis, N. S. *Science* **1990**, *250*, 1118.
- (8) Morris, R. B.; Franta, D. J.; White, H. S. *J. Phys. Chem.* **1987**, *91*, 3559.
- (9) Norton, J. D.; White, H. S.; Feldberg, S. W. *J. Phys. Chem.* **1990**, *94*, 6772.
- (10) Smith, C. P.; White, H. S. *Anal. Chem.* **1993**, *65*, 3343.
- (11) Watkins, J. J.; White, H. S. *Langmuir* **2004**, *20*, 5474.
- (12) Conyers, J. L., Jr.; White, H. S. *Anal. Chem.* **2000**, *72*, 4441.
- (13) Chen, S.; Kucernak, A. *J. Phys. Chem. B* **2002**, *106*, 9396.
- (14) Shao, Y.; Mirkin, M. V.; Fish, G.; Kokotov, S.; Palanker, D.; Lewis, A. *Anal. Chem.* **1997**, *69*, 1627.
- (15) Pendley, B. D.; Abruña, H. D. *Anal. Chem.* **1990**, *62*, 782.
- (16) (a) Fan, F.-R. F.; Bard, A. J. *Science* **1995**, *267*, 871. (b) Fan, F.-R. F.; Kwak, J.; Bard, A. J. *J. Am. Chem. Soc.* **1996**, *118*, 9669.
- (17) Chen, S.; Kucernak, A. *J. Phys. Chem. B* **2004**, *108*, 13984.
- (18) (a) Bard, A. J.; Fan, F.-R. F.; Pierce, D. T.; Unwin, P. R.; Wipf, D. O.; Zhou, F. *Science* **1991**, *254*, 68. (b) Mirkin, M. V. *Anal. Chem.* **1996**, *68*, 177 A.
- (19) Abbou, J.; Demaille, C.; Druet, M.; Moiroux, J. *Anal. Chem.* **2002**, *74*, 6355.
- (20) Sun, P.; Zhang, Z.; Guo, J.; Shao, Y. *Anal. Chem.* **2001**, *73*, 5346.
- (21) Gardner, C. E.; Macpherson, J. V. *Anal. Chem.* **2002**, 576A.
- (22) (a) Lay, M. D.; Sorenson, T. A.; Stickney, J. L. *J. Phys. Chem. B* **2003**, *107*, 10598. (b) Güell, A. G.; Díez-Pérez, I.; Gorostiza, P.; Sanz, F. *Anal. Chem.* **2004**, *76*, 5218.
- (23) Wightman, R. M. *Science* **2006**, *311*, 1570.
- (24) Lanyon, Y. H.; De Marzi, G.; Watson, Y. E.; Quinn, A. J.; Gleeson, J. P.; Redmond, G.; Arrigan, D. W. M. *Anal. Chem.* **2007**, *79*, 3048.
- (25) (a) Fologea, D.; Gershow, M.; Ledden, B.; McNabb, D. S.; Golovchenko, J. A.; Li, J. *Nano Lett.* **2005**, *5*, 1905. (b) Fologea, D.; Gershow, M.; Uplinger, J.; Thomas, B.; McNabb, D. S.; Li, J. *Nano Lett.* **2005**, *5*, 1734. (c) Chen, P.; Gu, J.; Brandin, E.; Kin, Y.-R.; Wang, Q.; Branton, D. *Nano Lett.* **2004**, *4*, 2293. (d) Storm, A. J.; Chen, J. H.; Ling, X. S.; Zandbergen, H. W.; Dekker, C. *Nat. Mater.* **2003**, *2*, 537. (e) Hinds, B. J.; Chopra, N.; Rantell, T.; Andrews, R.; Gavalas, V.; Bachas, L. G. *Science* **2004**, *303*, 62. (f) Ito, T.; Sun, L.; Henriquez, R. R.; Crooks, R. M. *Acc. Chem. Res.* **2004**, *37*, 937. (g) Harrell, C. C.; Kohli, P.; Siwy, Z.; Martin, C. R. *J. Am. Chem. Soc.* **2004**, *126*, 15646. (h) Heins, E. A.; Siwy, Z. S.; Baker, L. A.; Martin, C. R. *Nano Lett.* **2005**, *5*, 1824. (i) Siwy, Z.; Heins, E.; Harrell, C. C.; Kohli, P.; Martin, C. R. *J. Am. Chem. Soc.* **2004**, *126*, 10850.
- (26) Zoski, C. G. *Electroanalysis* **2002**, *14*, 1041.
- (27) Watkins, J. J.; Zhang, B.; White, H. S. *J. Chem. Educ.* **2005**, *82*, 712.
- (28) Arrigan, D. W. M. *Analyst* **2004**, *129*, 1157.
- (29) Penner, R. M.; Heben, M. J.; Lewis, N. S. *Anal. Chem.* **1989**, *61*, 1630.
- (30) Huang, W.-H.; Pang, D.-W.; Tong, H.; Wang, Z.-L.; Cheng, J.-K. *Anal. Chem.* **2001**, *73*, 1048.
- (31) Hrapovic, S.; Luong, J. H. T. *Anal. Chem.* **2003**, *75*, 3308.
- (32) Slevin, C. J.; Gray, N. J.; Macpherson, J. V.; Webb, M. A.; Unwin, P. R. *Electrochem. Commun.* **1999**, *1*, 282.
- (33) Woo, D.-H.; Kang, H.; Park, S.-M. *Anal. Chem.* **2003**, *75*, 6732.

- (34) Ballesteros Katemann, B.; Schuhmann, W. *Electroanalysis* **2002**, *14*, 22.

was heated in an oven at 120 °C for ~15 min to dry the Ag epoxy. The end of the Au or Pt wire was electrochemically etched to a sharp point in 6 M NaCN/0.1 M NaOH solution following standard methods reported elsewhere.<sup>35</sup> Briefly, a 100–300 Hz ac voltage (~4 V amplitude) was applied between the Pt or Au wire and a large-area Pt electrode using an Agilent 33220A function/arbitrary generator. Bubbles formed at the metal/solution interface during electrochemical etching; the applied voltage was removed immediately upon cessation of bubbling and the sharpened wire was washed with H<sub>2</sub>O. Pt tips were further sharpened, as described in the text below, using a custom-designed waveform generator. A circuit diagram and construction details of the waveform generator are available, free of charge, from the authors upon request.

The sharpened end of the Pt or Au wire was inserted into a glass capillary, leaving ~3 mm between the tip and the end of the glass tube. The wire was then sealed into the glass tube by slowly softening the capillary in a H<sub>2</sub>–O<sub>2</sub> flame. An optical microscope was used to frequently check the quality of the seal during this process (e.g., to ensure that no air bubbles became trapped near the metal tip). After obtaining an acceptable seal, the top of the W rod is secured to the glass capillary with epoxy (Dexter). Rough polishing to remove a large portion of the glass (i.e., leaving ~100 μm between the metal tip and the outside edge of the capillary) is accomplished using fine sand paper or emery cloth. Final polishing to expose the Pt or Au disk is performed using a Buehler Microcloth polishing pad mounted on a green glass plate with the aid of an electrical circuit as described in Results and Discussion. The polishing cloth was wetted with a slurry of 50-nm Al<sub>2</sub>O<sub>3</sub> particles and 0.02 M KCl.

**Electrochemical Apparatus.** A Chemclamp (Cornerstone Series) voltammeter–amperometer (Dagan Corp.) and a Princeton Applied Research 175 Universal Programmer were employed in both the voltammetric and conductivity measurements. The high-sensitivity preamplifier (0.05–1 nA/V) of the Chemclamp voltammeter–amperometer was used in all experiments and was contained in a Faraday cage during data acquisition. The electrochemical instrumentation was interfaced to a PC computer through a National Instruments (NI) PCI-6040 Multifunction I/O and NI-DAQ card and an NI BNC-2090, and voltammetric data were recorded using in-house virtual instrumentation written in NI LabVIEW 6.0. The *i*–*V* data were collected at 10<sup>4</sup> Hz and averaged over 10<sup>3</sup> points, with a noise level below a few hundred femtoamperes. A one-compartment, two-electrode cell was placed in the Faraday cage for all experiments. A Ag/Ag<sub>x</sub>O wire (1-mm diameter) or Ag/AgCl (3 M NaCl) electrode was used as a counter electrode in voltammetric measurements. Ag/AgCl electrodes were used to measure the conductivity of glass nanopore membranes.

**Microscopy.** SEM images were obtained using a LEO Leica S440 SEM. TEM images were obtained at the University of Utah Health Science Center (HSC) Core Research Facilities using a Hitachi H4000 TEM. Optical Images were acquired using an Olympus BX60 Optical Microscope. Atomic force microscopy (AFM) was performed with a Veeco AFM using a Nanoscope IIIa controller.

**Table 1. Melting/Softening Points and Linear Thermal Expansion Coefficients of Pt, Au, and Glasses**

material	melting/ softening point, °C	expansion coeff (25 °C), (× 10 <sup>6</sup> ) K <sup>−1</sup>	conductivity (Ω·m) <sup>−1</sup>
platinum <sup>a</sup>	1769	9	9.3 × 10 <sup>6</sup>
gold <sup>a</sup>	1064	14	4.4 × 10 <sup>7</sup>
soda lime glass	~700 <sup>b</sup>	9.3 <sup>d</sup>	~10 <sup>−14e</sup>
Pb doped glass	~600 <sup>c</sup>	9.5	~10 <sup>−18e</sup>

<sup>a</sup> All properties of metals from: Lide, D. R., Ed. *CRC Handbook of Chemistry and Physics*, 72nd ed.; CRC Press: Boca Raton, 1991. <sup>b</sup> www.dagan.com. <sup>c</sup> www.warneronline.com. <sup>d</sup> Data provided by the manufacturer. <sup>e</sup> Harper, C. A., Ed. *Handbook of Ceramics Glasses, and Diamonds*; McGraw-Hill: New York, 2001.

## RESULTS AND DISCUSSION

Fabrication of the Au and Pt nanodisk electrodes is the initial step in the fabrication of glass nanopore electrodes and glass nanopore membranes. To this end, there are three key steps in preparing a nanometer-scale electrode. First, it is critical to obtain very sharp tips since the ability to fabricate small electrodes is ultimately limited by the radius of curvature of the tip of the embedded wire. As a rule of thumb, we have observed that the radius of a disk in the 10–50-nm range, and consequently, the radius of a glass nanopore of similar dimensions, cannot be significantly smaller than the radius of curvature of the initial metal tip. This places a premium on the ability to generate very sharp wires (e.g., tips with radii less than ~10 nm). Second, the metal wire must be embedded in glass, which requires heating the capillary to its softening point. This process can easily lead to deformation of the tip. Thus, we have found, as expected, that embedding Pt wires (mp 1769 °C) in glass is much simpler than embedding Au (mp 1064 °C), the latter tending to melt unless great care and skill are used in heating the glass just to its softening point (600–700 °C; a list of relevant properties of the metals and glasses is presented in Table 1). Third, excess glass must be removed by carefully polishing to expose the Au or Pt disk. The most critical component of this final step is the ability to stop polishing precisely at the moment that a disk of desired radius is exposed. Due to the conical shape of the sharpened metal tips, even slight overpolishing results in electrodes with radii much larger than desired. To overcome the limitations inherent in the mechanical polishing process, a feedback circuit employing a high-impedance MOSFET switch is utilized. This device is designed to alert the experimentalist, in real time during polishing that a disk of preselected radius has been obtained. With these general concepts in mind, and with the objective of presenting a reproducible procedure that can be adapted by others, we present detailed descriptions of each fabrication step, with an emphasis on characterization of the intermediate structures.

**Electrochemical Etching of Au and Pt Tips.** Figure 2 shows electron micrographs of Pt and Au tips after etching in 6 M NaCN/0.1 M NaOH (see Experimental Section). Although similar conditions are used (~180 Hz, 3.6 V for Pt, 4.5 V for Au), the radius of curvature of Au tips (<20 nm) is significantly smaller than that of Pt (~50 nm).

In order to refine our fabrication procedure, we systematically investigated several parameters that influence the tip shape and structure. First, larger diameter metal wires result in larger cone

(35) (a) Melmed, A. J. *J. Vac. Sci. Technol., B* **1991**, 9, 601. (b) Melmed, A. J.; Carroll, J. J. *J. Vac. Sci. Technol., A* **1984**, 2, 1388.



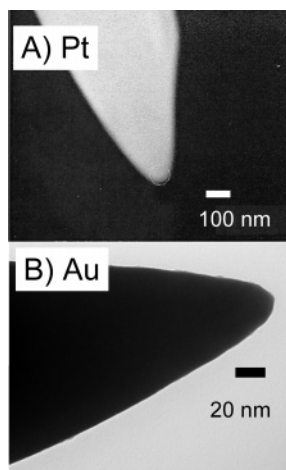


**Figure 2.** Electron microscopy images of (A) Pt (SEM) and (B) Au (TEM) wires after etching in 6 M NaCN/0.1 M NaOH.

angles near the tip. For example, etching a 25- $\mu\text{m}$ -diameter Pt wire yields tips with half-cone angles of  $8.5 \pm 1^\circ$ , while etching a 100- $\mu\text{m}$ -diameter Pt wire yields tips with half-cone angles of  $14 \pm 1^\circ$ . The ability to control the cone angle of the tip is of practical utility, as the transport resistance of the glass nanopores is sensitive to this parameter.<sup>2</sup> Second, the surface roughness of the etched metal tips, especially for Pt, is very dependent on the frequency of the applied ac voltage. Higher frequencies yield significantly smoother surfaces. However, the frequency of the etching voltage must be less than 1000 Hz in order to produce sharp tips. We have found empirically that a frequency range of 110–300 Hz yields tips that are satisfactory for producing nanodisks. The Supporting Information file provides data showing the effect of wire size and etching frequency on tip structure.

**Electrochemical Sharpening of Pt Tips.** Nanodisk electrodes with radii between 30 and 100 nm can be fabricated using Pt tips prepared as described in the previous section. To fabricate even smaller Pt electrodes, the procedure described by Libioulle et al.<sup>36</sup> for sharpening Pt tips for use in scanning tunneling microscopy was adopted, with a few modifications. Figure 3A shows a U-shaped electrochemical cell that is employed for this purpose. This cell has a large reservoir on the left-hand side that is used to position the air–solution (0.1 M  $\text{H}_2\text{SO}_4$ ) interface in the horizontal glass tube at right. The end of an etched Pt tip is inserted orthogonally across the meniscus of the 0.1 M  $\text{H}_2\text{SO}_4$  within the horizontal glass tube. A pulsed voltage waveform is then applied to electrochemically sharpen the tip further. Following Libioulle et al., we applied a 4-kHz, 15-V, 16- $\mu\text{s}$  pulse waveform for 1 s with a home-built waveform generator, followed by a dc potential of  $-1.1$  V for 10 s to remove any  $\text{PtO}_x$ . The voltage program as a function of time is represented in Figure 3B. Repetition of the program was carried out three times in succession to obtain sufficiently sharp tips for electrode fabrication.

Figure 4 shows a TEM image of a typical Pt tip sharpened by the procedure outlined above. The radius of curvature of the tip is  $\sim 2$  nm, and the surface appears free from oxide deposits (which are readily observable when the negative dc potential is not applied for 10 s as the final step). TEM characterization indicates that the majority of Pt tips processed using the program in Figure 3B have radii of  $<10$  nm.

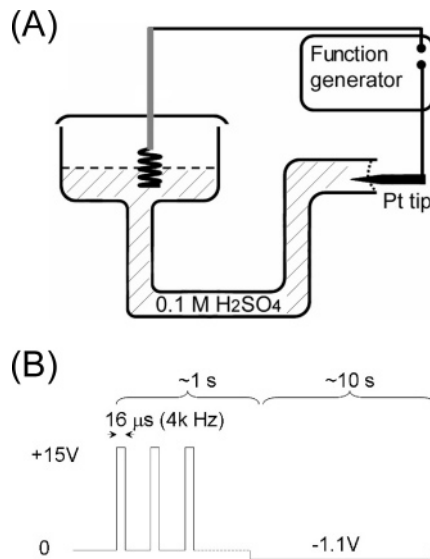


**Figure 3.** (A) Schematic of the cell and (B) pulse waveform for preparing ultrasharp Pt tips.

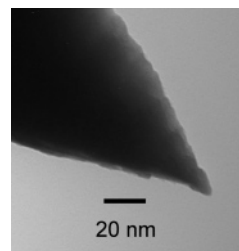


**Figure 4.** High-resolution TEM image of a Pt tip following sharpening in 0.1 M  $\text{H}_2\text{SO}_4$ .

**Sealing Pt and Au Tips in Glass.** Two primary conditions must be met in order to seal the metal into a glass capillary without destroying the ultrasharp Pt and Au tips. First, the thermal expansion coefficient of the glass should be equal to or greater than that of the metal to prevent crevice formation upon cooling. Second, the sealing temperature must be much lower than the melting point of the metal in order to avoid changes in tip shape. Thus, the softening temperature of the glass should be significantly lower than the melting point of the metal.

Table 1 lists the melting points and linear expansion coefficients of the metals and glasses used in this study. The melting point of Pt ( $\sim 1770^\circ\text{C}$ ) is  $\sim 1000^\circ\text{C}$  higher than the softening point of either soda lime or Pb-doped glass, and the expansion coefficients of Pt and both glass types are very closely matched. These conditions indicate that Pt is well suited for sealing in either type of capillary. Although Au has a significantly higher thermal expansion coefficient than either soda lime or lead glass and a melting point ( $\sim 1060^\circ\text{C}$ ) that is only 300–400  $^\circ\text{C}$  higher than the glass softening points, we have successfully sealed Au in Pb-doped glass capillaries (as judged from the voltammetric response). With extra care and patience, Au tips can be sealed into soda lime glass, but with a lower success rate. Regardless of the glass chosen, care must be taken during the sealing process to avoid melting the tip.

Optical images of both Pt and Au tips before and after sealing into glass capillaries are presented in the Supporting Information file. No noticeable damage to the sealed tips can be resolved in these images.

(36) Libioulle, L.; Houbion, Y.; Gilles, J.-M. *Rev. Sci. Instrum.* **1995**, *66*, 97.

### Polishing Glass Shrouded Metal Nanodisk Electrodes.

To aid hand polishing, a high-input impedance (MOSFET)-based electrical continuity circuit is used to signal the exposure of a metal disk of preselected size during polishing. Experimentally, the electrical resistance between the Pt or Au wire sealed in glass and the felt polishing cloth (wetted with a KCl solution containing 50-nm  $\text{Al}_2\text{O}_3$  particles and connected to the external circuit with a metal clip) is measured. The successful implementation of this strategy hinges on designing the circuit such that the user is alerted at precisely the moment a Pt or Au disk of desired radius is obtained during polishing. To this end, we undertook an analysis of the electrical resistance as function of the thickness of the glass above the tip during polishing. The combined resistance of the Pt or Au wire, the glass, and the electrolyte-wetted polishing cloth is referred to here as the resistance of the polishing circuit.

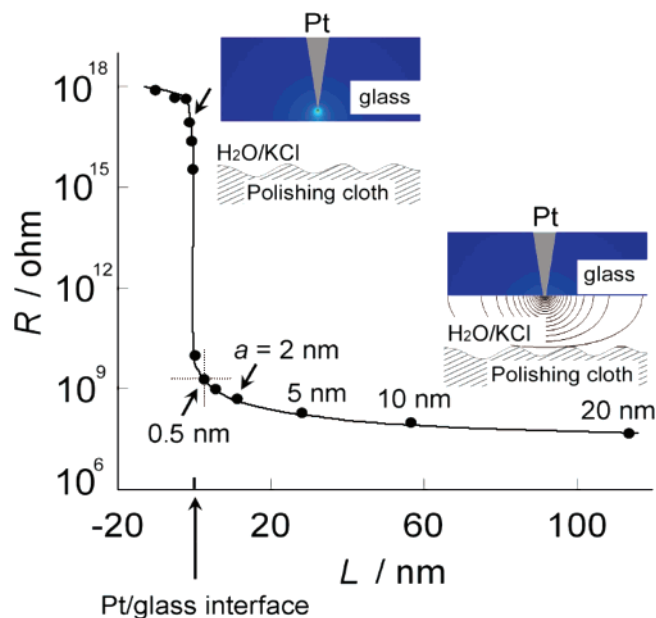
The total resistance between the Pt or Au wire embedded in the glass and the polishing cloth was computed using finite element simulations (Comsol Multiphysics, employing the "dc conductive media" mode). The electrical conductivity of glass used in the simulations was set at  $10^{-10} (\Omega\cdot\text{m})^{-1}$ , higher than that of soda lime or Pb-doped glasses (Table 1) but still 17 orders of magnitude lower than Pt or Au. Prior to exposure of the metal wire, the glass layer between the metal tip and the polishing cloth is by far the dominant resistance and, in fact, is immeasurably large; thus, the resistance of the solution can be ignored. Upon exposure of the tip, the spreading resistance at the nanodisk/electrolyte interface becomes the dominant resistance and is computed using the equation<sup>37</sup>

$$R = (4\kappa a)^{-1} \quad (1)$$

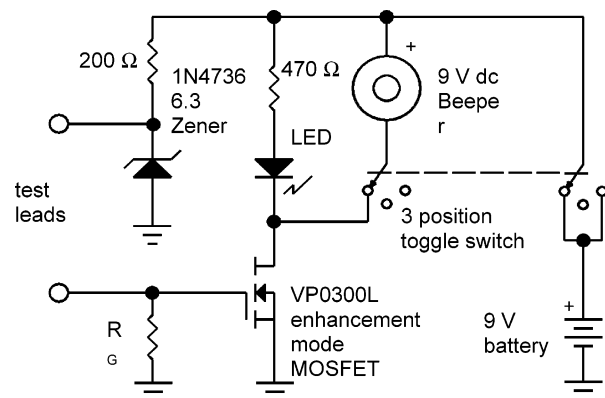
where  $\kappa$  is the conductivity of the 0.02 M KCl solution ( $\kappa \sim 0.14 (\Omega\cdot\text{m})^{-1}$ ) on the polishing cloth and  $a$  is the radius of the metal disk. Since the voltage drop in the electrolyte occurs over a very small distance ( $\sim 10a$ ), it is not necessary to precisely model the electrolyte layer thickness on the polishing cloth. A semi-infinite layer of polishing solution is assumed. This is clearly an approximation, as the thickness of this layer is varied as the glass/metal surface moves across the poorly defined surface of the polishing felt. Nevertheless, the results below show that the use of this approximation yields numerical predictions that allow the radius of the disk to be controlled with reasonable accuracy and precision.

Figure 5 shows a plot of the logarithm of the polishing circuit resistance ( $\log R (\Omega)$ ) as a function of the polishing depth,  $L$  (nm). The value of  $L = 0$  corresponds to the position of the end of the sharpened metal tip. Thus, negative values of  $L$  correspond to the thickness of the glass layer before the tip is exposed, while positive values correspond to the thickness of the glass removed following tip exposure. A simple geometric analysis can be used to convert  $L$  values to the exposed disk radius (selected values of  $a$  are shown in Figure 5). Thus, in principle, measurement of the polishing circuit resistance enables determination of the size of the metal disk during polishing.

The MOSFET circuit shown in Figure 6 and described below, can be employed as a dc continuity tester to determine the



**Figure 5.** Resistance of a glass-sealed Pt disk electrode during polishing computed from finite-element simulations and eq 1. Insets depict the potential distribution before and after exposure of the Pt disk. Values of resistance corresponding to various disk radii ( $a$ ) are shown on the plot. The resistance calculations assume a polishing solution containing 0.02 M KCl.



**Figure 6.** Circuit diagram of the high-sensitivity electrical continuity tester. The gate resistance  $R_G$  (Table 2) is adjusted to signal the end of polishing when a nanodisk of preselected radius is obtained during polishing.

moment during polishing when the metal tip first becomes exposed. From the simulations in Figure 5, continuity is observed when  $R$  decreases from  $\sim 10^{18}$  (immeasurably large) to  $\sim 10^9 \Omega$ . A notable progression is  $R = 8.9 \text{ G}\Omega$  for  $a = 0.1 \text{ nm}$ ,  $4.5 \text{ G}\Omega$  for  $a = 0.2 \text{ nm}$ , and  $1.8 \text{ G}\Omega$  for  $a = 0.5 \text{ nm}$ . In the circuit described below, electrical continuity is defined when  $R = \sim 2 \text{ G}\Omega$ , corresponding to a metal nanodisk with a  $\sim 0.5 \text{ nm}$  (exposure of  $\sim 10$  metal atoms of  $0.15 \text{ nm}$  radius in a circular disk would meet this criterion).

The diagram of the MOSFET circuit used for polishing is shown in Figure 6. The signaling mechanism consists of a solid-state beeper and an LED, which are both connected between the +9-V battery terminal and the drain lead of a VL0300L MOSFET transistor. The source lead of this transistor is connected to the negative terminal of the battery. The test leads are connected such

(37) Bard, A. J.; Faulkner, L. R. *Electrochemical Methods: Fundamentals and Applications*; 2nd ed.; Wiley: New York, 2001.

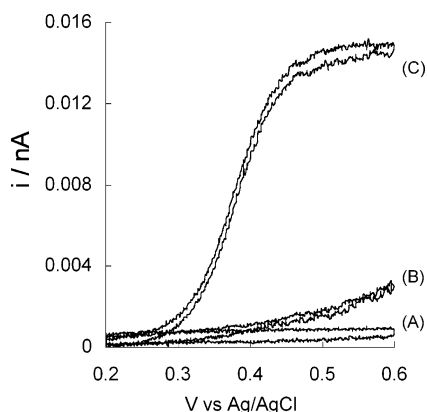


**Figure 7.** Voltammetric response of a Pt disk electrode in  $\text{CH}_3\text{CN}$  containing 5 mM Fc and 0.2 M  $\text{TBAPF}_6$  (A) before and (B) after tip exposure and (C) following sonication in ethanol (sweep rate,  $20 \text{ mV s}^{-1}$ ).

that the transistor acts as a switch in the circuit; when a complete circuit is created by a resistance of less than  $\sim 2 \text{ G}\Omega$  between the test leads, the beeper will sound and the LED will turn on. This is accomplished by attaching one test lead directly to the +9-V battery terminal and the other to the transistor gate via a gate resistor,  $R_G$ , of  $500 \text{ M}\Omega$  that is wired in series to the negative battery terminal. When the test resistance drops below  $\sim 2 \text{ G}\Omega$ , a  $\sim 1.5\text{-V}$  drop across the  $500\text{-M}\Omega$  resistor will activate the transistor. The enhancement mode FET is normally off, and therefore, the beeper and LED are normally off.

In operation, one test lead is connected to the W rod that contacts the Pt or Au wire embedded in the glass capillary, and the other test lead is bathed in the solution on the polishing cloth. When enough glass has been polished to just barely expose the Pt/Au tip, sufficient current will flow through the probe, causing a voltage drop across the  $500\text{-M}\Omega$  gate resistor, which activates the transistor.

We have observed that upon first exposure (or perhaps, upon *near* exposure) of the metal, an intermittent audio or LED signal occurs, which is likely due to capacitive currents associated with the thin glass layer or faradic reactions upon exposure of the first few metal atoms. An additional few seconds of polishing results in a continuous signal that is probably associated with oxidation or reduction of  $\text{H}_2\text{O}$  or other redox-active constituents of the electrolyte ( $\text{Cl}^-$ ,  $\text{O}_2$ ) that wet the polishing cloth. The charge-transfer reactions at the nanoelectrode and the test lead on the wetted polishing cloth are not well-defined. Although a more sensitive tester could be developed, such high-sensitivity devices are susceptible to false readings due to very small leakage currents through surface contamination of the test leads and through conduction or tunneling across the nanometer-thin glass layer just prior to exposing the tip.

The MOSFET circuit is housed in an inexpensive aluminum electronics project box (see Supporting Information). Importantly, the device is designed to measure extremely small currents; minute levels of contamination or moisture between the gate terminal and +9-V source will give a false signal. Therefore, it is recommended to avoid the use of a circuit board. The gate lead is soldered directly to the gate resistor and the plug for the test lead. After constructing the unit, the resistor body and transistor are cleaned with alcohol to minimize stray current paths. Test

leads are also kept as short as practical ( $\sim 10 \text{ cm}$ ) to ensure minimal leakage currents. Although the  $500\text{-M}\Omega$  gate resistor eliminates most problems with static buildup, the test leads are kept shorted together during storage. Static discharge from touching the test leads can potentially damage the transistor.

The radii of the exposed metal disks were determined by several means, including steady-state voltammetry, atomic force microscopy, conductance measurements (of the nanopore after removal of the metal), and electron microscopy (as previously described<sup>1</sup>). All nanodisk radii in our laboratory are measured by steady-state voltammetry, which is by far the least intensive method. Representative samples are also characterized by an additional method to establish correlations with the voltammetric measurements, ensuring mutual validity. In voltammetry, the radius of the nanodisk is assessed using the steady-state limiting current,  $i_d$ , for the oxidation of a soluble redox species through the equation<sup>38</sup>

$$i_d = 4nFDC^*a \quad (2)$$

In eq 2,  $n$  is the electron stoichiometry,  $F$  is Faraday's constant, and  $D$  and  $C^*$  are the diffusion coefficient and bulk concentration of the redox molecule, respectively. Values of  $a$  were determined by measuring  $i_d$  for the oxidation of 5.0 mM ferrocene (Fc;  $D = 2.5 \times 10^{-5} \text{ cm}^2 \text{ s}^{-1}$ ) in acetonitrile (supporting electrolyte 0.2 M  $\text{TBAPF}_6$ ).

Figure 7 shows the voltammetric response of a Pt disk electrode in 5.0 mM Fc/0.2 M  $\text{TBAPF}_6$  solution before tip exposure (A), immediately after the electrical circuit signaled exposure with intermittent beeping (B), and after sonicating the nanodisk in ethanol for  $\sim 20 \text{ s}$  (C). Prior to exposure of the metal tip, Figure 7A, there is a small charging current ( $\sim 0.5 \text{ pA}$ , Figure 7A) that corresponds, at least partially, to the stray capacitance of the instrument. This background capacitance is observed whether or not the metal nanodisk is exposed and appears even when the capillary and metal wire are removed entirely from the solution. Upon first continuous exposure of the Pt, the voltammetric curve, Figure 7B, shows an approximately exponential increase in current beginning near  $E^\circ$  (the thermodynamic redox potential). This current does not reach a diffusion-limited plateau. We speculate that this current arises from any combination of (1) conductance or tunneling across a very thin glass layer ( $< 1 \text{ nm}$ ) that remains above the Pt tip or (2) kinetically controlled oxidation of Fc at a subnanometer-radius nanodisk. A crude analysis assuming Butler–Volmer kinetics<sup>37</sup> for Fc oxidation with a heterogeneous electron-transfer rate constant of  $5 \text{ cm/s}$ <sup>6</sup> yields a Pt disk radius of  $\sim 0.4 \text{ nm}$  (Note: we are not claiming that the radius is  $0.4 \text{ nm}$ , but only that the electrochemical response in Figure 7B is consistent with this size). Figure 7C shows that a voltammetric response exhibiting a well-defined diffusion-limited current plateau is obtained after a brief sonication of the electrode (5 s). Sonication is believed to remove any remaining glass at the electrode surface, albeit in an uncontrolled fashion. The voltammetric response after sonication corresponds to a radius  $\sim 4 \text{ nm}$ .

Continuing polishing briefly beyond the intermittent beeping stage (until a continuous audio alert is obtained) results in

(38) Saito, Y. *Rev. Polarogr.* **1968**, *15*, 177.

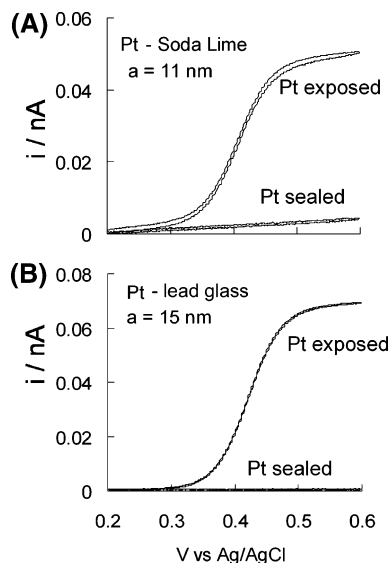


**Figure 8.** (a) Voltammetric responses of Pt nanodisk electrodes measured in  $\text{CH}_3\text{CN}/0.2 \text{ M TBAPF}_6$  containing  $5.0 \text{ mM Fc}$ . (A)  $11\text{-nm}$ -radius disk sealed in soda lime glass and (B)  $15\text{-nm}$ -radius disk sealed in Pb glass (sweep rate,  $20 \text{ mV s}^{-1}$ ).

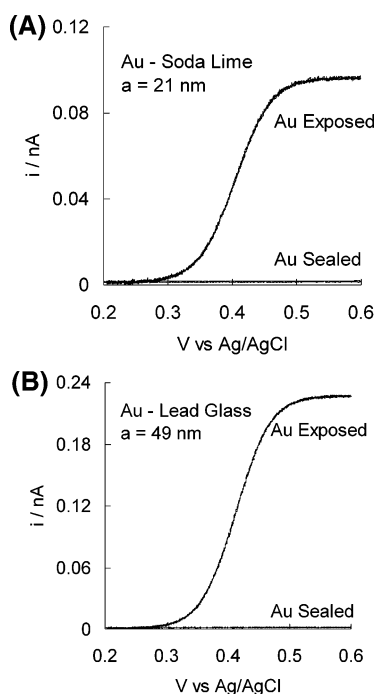


**Figure 9.** Voltammetric responses of Au nanodisk electrodes measured in  $\text{CH}_3\text{CN}/0.2 \text{ M TBAPF}_6$  containing  $5.0 \text{ mM Fc}$ . (A)  $21\text{-nm}$ -radius disk sealed in soda lime glass and (B)  $49\text{-nm}$ -radius disk sealed in Pb glass (sweep rate,  $20 \text{ mV s}^{-1}$ ).

electrodes that give well-defined voltammetry. The  $i$ - $V$  curves in  $5.0 \text{ mM Fc}$  solutions for two different Pt electrodes are presented in Figure 8. These electrodes were prepared using soda lime glass ( $a = 11 \text{ nm}$ , Figure 8A) and Pb-doped glass ( $a = 15 \text{ nm}$ , Figure 8B). Similar voltammetric responses were obtained for glass-shrouded nanodisks prepared using sharpened Au wires, Figure 9. Using the MOSFET circuit, we find that Pt nanodisks with radii ranging between  $10$  and  $30 \text{ nm}$  can be routinely prepared by the above method, the majority of which exhibit nearly ideal voltammetric behavior (similar to the examples presented herein). Au

**Table 2. Polishing Parameters and Nanodisk Electrode Fabrication Results**

desired disk radius (nm)	polishing set point $R$ ( $\text{M}\Omega$ )	gate resistance $R_g$ ( $\text{M}\Omega$ )	measured disk radius, nm ( $N^a$ )	range of disk radius (nm)
10	173	48.1	$7 \pm 4$ (10)	4–14
50	35	13.8	$35 \pm 19$ (6)	10–55
100	17.3	6.51	$61 \pm 16$ (7)	43–85
200	8.67	3.57	$102 \pm 31$ (6)	64–150

<sup>a</sup>  $N$ , number of electrodes. <sup>b</sup> All electrodes polished on cloth wetted with  $20 \text{ mM KCl}$ .

nanodisk electrodes with radii less than  $100 \text{ nm}$  can also be routinely prepared by the above method, but we find the ability to reliably produce electrodes in the  $10$ – $50\text{-nm}$  range to be significantly lower than for Pt. A possible reason is that some melting of the Au tip occurs as it is sealed in the glass capillary. Optical micrographs of Au tips sealed in glass (see Supporting Information) would not be able to resolve this level of structural change.

Close examination of Figure 8 reveals a difference in the voltammetric response of the two Pt electrodes prepared using soda lime and Pb-doped glass capillaries. The  $i$ - $V$  response of the Pt electrode shrouded in soda lime glass exhibits a significantly larger linear background slope ( $75 \text{ pA/V}$ ) than that of the Pb-doped glass (immeasurably small). This slope is not due to a poor glass/metal seal, but instead reflects the steady-state flux of  $\text{Na}^+$  within the bulk soda lime glass. This supposition is supported by  $i$ - $V$  measurements in which a Pt wire was sealed entirely in soda lime glass (no polishing), as shown in Figures 8. The slopes of the  $i$ - $V$  curves of these electrodes at any time during polishing, but before exposure, are indistinguishable. The conduction process due to the transport of  $\text{Na}^+$  within the glass is thus superimposed on the voltammetric response for Fc oxidation. For example, in Figure 8A the  $i$ - $V$  curve for the sealed Pt shows significantly greater background current than the corresponding  $i$ - $V$  curve in Figure 8B, for an electrode sealed in Pb-doped glass. This effect is readily detectable using the smallest electrodes due to the high current sensitivity used in recording the data. The reproducible absence of an ohmic background when using Pb-doped capillaries is consistent with the much lower ionic conductivity of Pb-doped glass relative to soda lime glass (see Table 1).

The value of  $R_G$  in the circuit of Figure 6 can varied in order to activate the MOSFET transistor for different selected values of  $R$ , which allows electrodes of different desired radius to be fabricated. For instance, a Pt disk of  $50 \text{ nm}$  radius corresponds to  $R = 35 \text{ M}\Omega$ , eq 1. To signal the presence of a  $50 \text{ nm}$  radius disk during polishing, a gate resistance of  $R_G = 6.51 \text{ M}\Omega$  is employed. Table 2 lists appropriate values of  $R_G$  required to activate the circuit in producing electrodes with  $a = 10, 50, 100$ , and  $200 \text{ nm}$ . Polishing is immediately ceased upon indication of selected radius either by the LED or audio signal.

Figure 10 shows a plot of the measured radius versus the preselected or desired electrode radius, experimentally chosen using eq 1 to compute the value of  $R$  corresponding to  $a$  and varying  $R_G$  as described above. Values of  $R$ ,  $R_G$ , and tabulated results (e.g., range of observed  $a$ ) are presented in Table 2. All



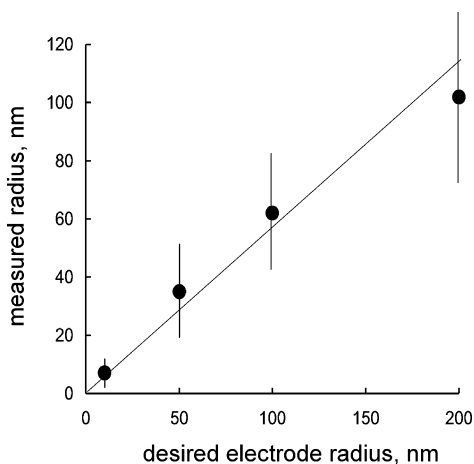


**Figure 10.** Measured radius vs desired radius of Pt disks. The desired radius was chosen by varying  $R_G$  in the MOSFET circuit shown in Figure 6. Values of  $R_G$  for different disk radius are listed in Table 2.

polishing was performed using a 0.02 M KCl solution. Admittedly, while the data in Figure 10 indicate that the precision in obtaining nanodisk electrodes of desired radius ( $\sim\pm 30\%$ ) is not ideal, the results indicate that the methodology using the MOSFET circuit allows rough control over the disk radius in the 10–200-nm range. Our laboratory has prepared several hundreds of Pt and Au nanodisk electrodes over the course of the past 2 years, without attempting to control the radius of the disk by varying  $R_G$ . The data presented in Figure 10 were collected by a single individual in order to test the viability of using electrical feedback to closely control the disk size. The linearity of the plot is very promising in this respect. Further refinement of the method is currently underway.

As previously discussed, electron microscopy has been used to measure the radii of our Pt nanodisk electrodes (as well as nanopore electrodes synthesized from nanodisks, see below). In general, we find good agreement between SEM-determined radii and voltammetric results for electrodes in which  $a$  is  $>80$  nm. We have been unable to obtain well-resolved images of smaller disks. In the following sections, however, we report AFM imaging and conductivity measurements of nanopore electrode orifices that were prepared from the nanodisk electrodes, noting that the results are in excellent agreement.

**Glass Nanopore Electrodes.** The glass nanopore electrode (see Figure 1B) is fabricated by etching the Pt or Au nanodisk electrode in a 20%  $\text{CaCl}_2$  solution, using a  $\sim 5$ -V amplitude ac voltage at a frequency of 60 Hz. The preparation, characterization, and surface chemical modification of these nanostructures have been previously detailed in reports from our laboratory<sup>1–4</sup> and are, thus, only briefly discussed here. The removal of Pt during etching creates a conical-shaped pore, the depth of which is controlled by varying the etching time. The essential difference in the voltammetric behavior of a Pt nanopore electrode with respect to a nanodisk electrode is a notable decrease in the diffusion-limited current. This reduction is a consequence of the larger mass-transfer resistance of the pore and, therefore, scales with pore size. Figure 11 shows the voltammetric responses of a 86-nm-radius Pt disk electrode and the corresponding glass nanopore electrode in 5.0 mM Fc. This particular nanopore resulted from

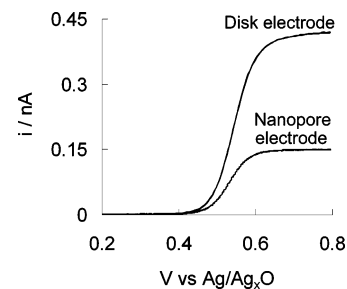


**Figure 11.** Voltammetric response of a 86-nm-radius nanodisk electrode and the corresponding nanopore electrode in  $\text{CH}_3\text{CN}$  containing 5.0 mM Fc and 0.2 M TBAPF<sub>6</sub>.

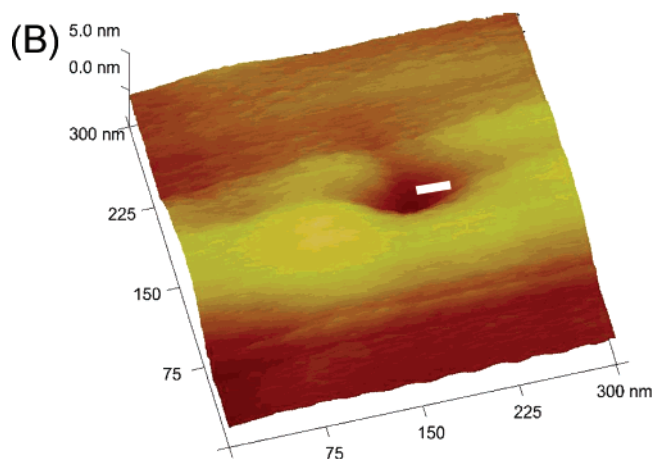
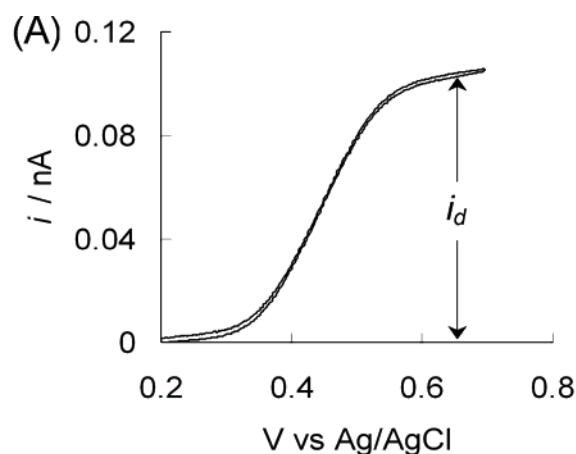


**Figure 12.** (A) Voltammetric response of a 23-nm-radius Pt disk electrode in  $\text{CH}_3\text{CN}$  containing 5.0 mM Fc and 0.2 M TBAPF<sub>6</sub>. (B) AFM image of the orifice after the Pt is partially removed from the electrode in part (A). A 23-nm scale bar is shown across the nanopore.

etching the Pt to a depth of  $\sim 250$  nm, as determined from the dependence of the limiting current on the ratio between the pore depth and the radius of the orifice ( $d/a$ ).<sup>2</sup> The  $\sim 65\%$  decrease in limiting current upon formation of the pore is consistent with published numerical simulations.<sup>2</sup>

Figure 12 shows (A) the voltammetric response of a Pt nanodisk electrode that was used to prepare a nanopore electrode and (B) an AFM image of the orifice of a nanopore electrode that resulted from etching this nanodisk electrode, using the procedure outlined above. The Pt nanodisk radius was determined to be 23 nm from measurement of the diffusion-limited current (Figure 12A). A 23-nm scale bar is shown on the AFM image, illustrating the voltammetric measurement is in excellent agreement with the



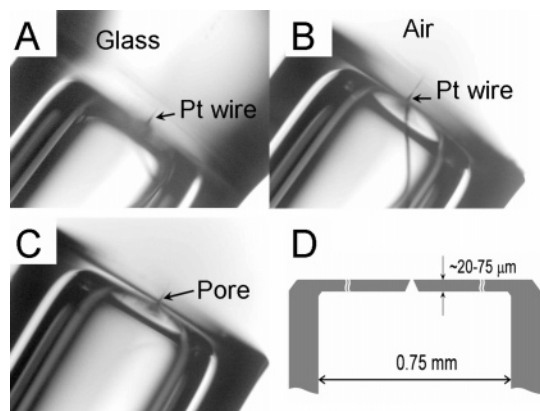


**Figure 13.** Optical images during the preparation of a glass nanopore membrane. (A) Pt sealed in bulk glass; (B) Pt sealed in glass membrane after polishing glass; (C) glass nanopore membrane after removal of Pt; (D) schematic of glass nanopore membrane showing nominal membrane dimensions. The small opening of the pore is not drawn to scale.

AFM image. This observation is consistent with earlier SEM studies of larger pores,<sup>1</sup> where the size of the nanopore and corresponding nanodisk electrode are similar. These results indicate that the voltammetric response yields accurate values of metal disk radii and that electrochemical etching of the Pt in  $\text{CaCl}_2$  does not remove a significant amount of glass from the walls of the resulting nanopore. Additional comparisons of the AFM- and voltammetrically measured orifice radii are presented in the Supporting Information file.

**Glass Nanopore Membranes.** The sealed metal wire can be removed entirely from the glass by a combined etching and mechanical process to make a glass membrane containing an individual conical-shaped nanopore. However, the fabrication of the glass nanopore membrane requires that the length of the Pt wire sealed in the glass capillary does not exceed  $\sim 100\ \mu\text{m}$ . Sealing very short lengths ( $25\text{--}50\ \mu\text{m}$ ) of the sharpened end of a Pt wire is accomplished using a specialized procedure. First, the tip is positioned at the middle of the glass capillary to avoid touching of the glass walls while the glass is being heated in the  $\text{H}_2$  torch. Initially, the Pt is positioned  $>0.5\ \text{cm}$  from the end of the glass capillary while the end of the capillary is heated. As the capillary softens and collapses, the interior surface becomes very flat. At this point, the glass capillary is removed from the flame and the Pt tip is positioned as close as possible toward the sealed end of the capillary, taking care to avoid physical touching of the glass surface by monitoring progress with an optical microscope. The capillary is then placed back into the lower, cooler part of the flame to continue softening the glass with constant visual inspection of the interior flat surface. As the glass continues to soften in the flame, it eventually retracts and contacts the sharp Pt tip. This contact is observed by eye (with considerable practice) in real time by the sudden appearance of a spot at the point of contact. The capillary, with Pt tip sealed at the end, is immediately removed from the flame and allowed to cool. The sealed end of the capillary is inspected by optical microscopy ( $40\times$  magnification) to ensure that the end of the tip is embedded in glass.

The capillary is polished using the MOSFET circuit to create a Pt nanodisk electrode, the size of which can be controlled as described above. The Pt is then electrochemically etched in  $\text{CaCl}_2$

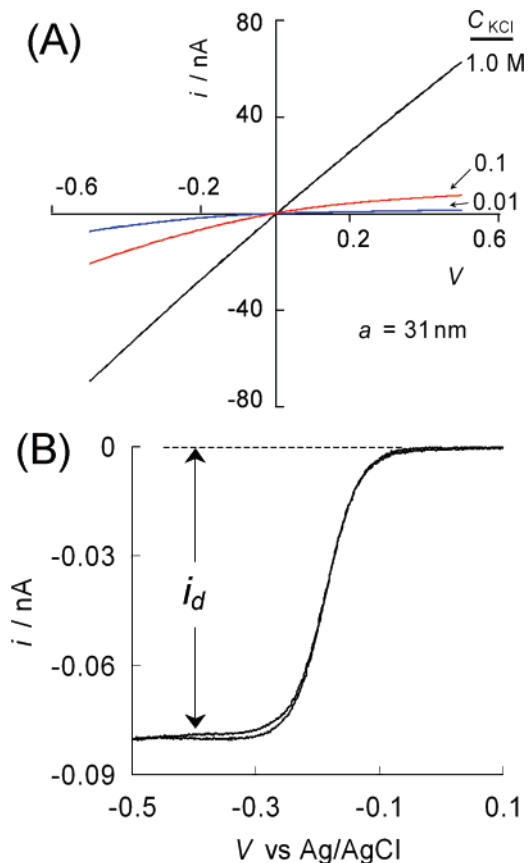


**Figure 14.** (A)  $i$ - $V$  curves corresponding to a glass nanopore membrane as a function of KCl concentration (scan rate,  $100\ \text{mV s}^{-1}$ ). (B) Voltammetric response of the corresponding Pt nanodisk (prior to removal of the Pt to create the nanopore membrane) in a  $10.0\ \text{mM Ru(NH}_3)_6\text{Cl}_3$  solution containing  $1\ \text{M KCl}$  (scan rate,  $20\ \text{mV s}^{-1}$ ). The pore orifice radius, as determined from the slope of the  $i$ - $V$  curve, eq 3, in part A for the  $1\ \text{M KCl}$  solution, is equal to  $31\ \text{nm}$ . The Pt disk radius, as determined from the voltammetric limiting current, eq 2, in part B is equal to  $32\ \text{nm}$ .

to remove as much of the Pt wire as possible from the glass. The remaining Pt can readily be removed from the glass at this point by gently twisting the W wire attached to the Pt inside the capillary. Figure 13 shows cross-sectional optical images of the following: (A) Pt tip sealed in glass; (B) the polished Pt nanodisk electrode; (C) the glass nanopore membrane after the tip is removed; and (D) a schematic drawing of the glass nanopore membrane showing the dimensions.

The radius of the small orifice of a glass nanopore membrane can be determined from the ionic resistance of the pore measured in a solution of known ionic conductivity.<sup>39</sup> The pore resistance is obtained from the slope of  $i$ - $V$  curves recorded by varying the potential between two Ag/AgCl electrodes positioned on opposite sides of the membrane. The relationship between the membrane resistance,  $R_p$ , and the small orifice radius,  $a_p$ , is given by<sup>5</sup>

$$R_p = \frac{1}{\kappa a_p} \left( \frac{1}{\pi \tan \theta} + \frac{1}{4} \right) \quad (3)$$

(39) Heins, E. A.; Siwy, Z. S.; Baker, L. A.; Martin, C. R. *Nano Lett.* **2005**, *5*, 1824.

where  $R_p$  is the resistance,  $\kappa$  is the conductivity of the solution, and  $\theta$  is the half-cone angle. The latter is equal to the half-cone angle of the Pt wire before it is sealed, which is measured by optical microscopy.

Figure 14B shows the voltammetric response of a Pt nanodisk electrode in a 10 mM  $\text{Ru}(\text{NH}_3)_6\text{Cl}_3$  solution containing 0.2 M KCl. The radius of the Pt disk is calculated from the diffusion-limited steady-state current to be 32 nm. Figure 14A shows the voltammetric response of the corresponding glass nanopore membrane in KCl solutions of varying concentration. The  $i$ - $V$  response in 1 M KCl is found to be nearly ohmic, with a slope corresponding to a small orifice radius of  $\sim 31$  nm, in good agreement with the value calculated from the electrochemical response. The  $i$ - $V$  response in KCl of low concentrations displays current rectification effects, similar to that reported by Wei et al. for current flow through tapered glass nanopipets.<sup>40</sup> Current rectification in conical nanopores has been recently reviewed by Siwy.<sup>41</sup> A detailed analysis of the rectification in the glass nanopore membranes is currently in progress and will be reported elsewhere.

## CONCLUSIONS

We have presented a benchtop method of fabricating glass sealed disk-shaped Pt and Au nanoelectrodes, glass nanopore electrodes, and glass nanopore membranes. The methods are readily implemented with common laboratory equipment and materials, and simple electronics. Pt electrodes with radii as small as 10 nm and Au electrodes with radii less than 100 nm can be fabricated with good reproducibility. These electrodes exhibit

nearly ideal voltammetric behavior and are chemically and structurally robust. We anticipate that they will find applications in electroanalyses and fundamental studies of electron-transfer reactions. The nanodisk electrodes are intermediate structures in the fabrication of glass nanopore electrodes and glass nanopore membranes. We have shown, using AFM imaging and conductivity measurements, that the orifice radii of these latter structures are consistent with the radii of the nanodisks from which they are prepared.

## ACKNOWLEDGMENT

We thank Mrs. Nancy Chandler, University of Utah Core Research Facilities, Dr. Di Wu, University of Utah physics, for their assistance in the TEM/SEM imaging, and Mr. Changwei Xiong, for his help in the optical microscopy imaging. B.Z. thanks the ACS Division of Analytical Chemistry, and the Society for Analytical Chemists of Pittsburgh (SACP), for a graduate summer research fellowship. This research was supported in part by the National Institutes of Health, the National Science Foundation, and the Defense Advanced Research Project Agency (FA9550-06-C-000C).

## SUPPORTING INFORMATION AVAILABLE

Additional AFM images or nanopore orifices, optical images of sealed Au and Pt wires, and the dependencies of wire diameter and polishing frequency. This material is available free of charge via the Internet at <http://pubs.acs.org>.

Received for review March 27, 2007. Accepted May 16, 2007.

AC070609J

(40) Wei, C.; Bard, A. J.; Feldberg, S. W. *Anal. Chem.* **1997**, *69*, 4627.

(41) Siwy, Z. S. *Adv. Funct. Mater.* **2006**, *16*, 735.